

Article

Experimental Study to Analyze Feasibility of a Novel Panelized Ground-Source Thermoelectric System for Building Space Heating and Cooling

Rui Miao ¹, Xiaouu Hu ¹, Yao Yu ^{1,*}, Qifeng Zhang ², Zhibin Lin ¹, Abdulaziz Banawi ¹
and Ahmed Cherif Megri ³

¹ Department of Civil, Construction and Environmental Engineering, North Dakota State University, Fargo, ND 58102, USA; rui.miao@ndsu.edu (R.M.); xiaoou.hu@ndsu.edu (X.H.); zhibin.lin@ndsu.edu (Z.L.); abdulaziz.banawi@ndsu.edu (A.B.)

² Department of Electrical and Computer Engineering, North Dakota State University, Fargo, ND 58102, USA; qifeng.zhang@ndsu.edu

³ Department of Civil, Environmental and Architectural Engineering, North Carolina A&T State University, Greensboro, NC 27411, USA; acmegri@ncat.edu

* Correspondence: yao.yu@ndsu.edu; Tel.: +1-701-231-8822

Abstract: A thermoelectric module is a device that converts electrical energy into thermal energy through a mechanism known as the Peltier effect. A Peltier device has hot and cold sides/substrates, and heat can be pumped from the cold side to the hot side under a given voltage. By applying it in buildings and attaching it to building envelope components, such as walls, as a heating and cooling device, the heating and cooling requirements can be met by reversing the voltage applied on these two sides/substrates. In this paper, we describe a novel, panelized, ground source, radiant system design for space heating and cooling in buildings by utilizing the Peltier effect. The system is equipped with water pipes that are attached to one side of the panel and connected with a ground loop to exchange heat between the cold/hot sides of the thermoelectric module and the underground region. The ground loop is inserted in boreholes, similar to those used for a vertical closed-loop Ground Source Heat Pump (GSHP) system, which could be more than a hundred meters deep. Experiments were conducted to evaluate the feasibility of the developed panel system applied in buildings. The results show that: (1) the average cooling Coefficients Of Performance (COP) of the system are low (0.6 or less) even though the ground is used as a heat sink, and thus additional studies are needed to improve it in the future, such as to arrange the thermoelectric modules in cascade and/or develop a new thermoelectric material that has a large Seebeck coefficient; and (2) the developed system using the underground region as the heat source has the potential of meeting heating loads of a building while maintaining at a higher system coefficient of performance (up to ~3.0) for space heating, compared to conventional heating devices, such as furnaces or boilers, especially in a region with mild winters and relatively warm ground.

Keywords: thermoelectric module; Peltier effect; ground source heat pump; building



Citation: Miao, R.; Hu, X.; Yu, Y.; Zhang, Q.; Lin, Z.; Banawi, A.; Megri, A.C. Experimental Study to Analyze Feasibility of a Novel Panelized Ground-Source Thermoelectric System for Building Space Heating and Cooling. *Energies* **2022**, *15*, 209. <https://doi.org/10.3390/en15010209>

Academic Editors:
Gianpiero Colangelo
and Luisa F. Cabeza

Received: 23 November 2021

Accepted: 19 December 2021

Published: 29 December 2021

Publisher's Note: MDPI stays neutral with regard to jurisdictional claims in published maps and institutional affiliations.



Copyright: © 2021 by the authors. Licensee MDPI, Basel, Switzerland. This article is an open access article distributed under the terms and conditions of the Creative Commons Attribution (CC BY) license (<https://creativecommons.org/licenses/by/4.0/>).

1. Introduction

According to the United Nations Environmental report, building construction (commercial and residential) and operations accounted for the largest share of global energy use (38%) with totally 144 exajoules [1], typically including approximately 40% energy consumption for space cooling and heating [2]. Investment in the energy efficiency of buildings continues to climb and reached more than USD 180 billion in 2020 [1]. Globally, fossil fuels, especially coal [3], are still the most frequently used energy sources (80%). The concerns around energy usage in buildings have been more focused in the last decades, and thus developing a new, high efficiency system with the goal of minimizing the use of fossil fuels

becomes the main duty in the future. For example, in 2020, the energy efficiency investment in buildings increased by 11% globally, and green building certifications increased by 13.9% compared to 2019 [1].

A ThermoElectric Module (TEM) is a device that converts electrical energy into thermal energy, known as the Peltier effect. A Peltier device has hot and cold sides/substrates (Figure 1a), and heat can be pumped from the cold side to the hot side under a given voltage. The TEM technology has advantages of reliability, compactness, noiselessness, mechanical stability, no working fluid required, and light weight [4,5]. Due to the unique advantages, this technology has been developed for multiple applications, such as small-scale devices like CPUs (Central Processing Units), portable refrigerators, medical applications, laboratory equipment cooling, etc. [6–10]. For example, Gao and Rowe [7] evaluated the cooling performance of a thermoelectric refrigerator, and Sabah et al. [8] designed and built an affordable solar thermoelectric refrigerator, which uses a TEM system to create heat and cold for the Bedouin people living in remote parts of Oman. In these studies [7,8], the TEM refrigerator systems demonstrated a good performance, and TEM was shown by Putra et al. [9] to be an effective cooling source for cryosurgery. For large-scale applications, such as for buildings' energy systems, it is rarely used but has significant potential [5,11]. In recent years, the idea of applying TEM systems for heating and cooling purposes in buildings has received significant attention, such as their integration with building envelopes [11–13] and their use for de-humidification [14,15], for providing heat to clothes dryers [16], and for space heating/cooling in buildings [6,17–19], as well as the development of new TEM heating/cooling units [20–25].

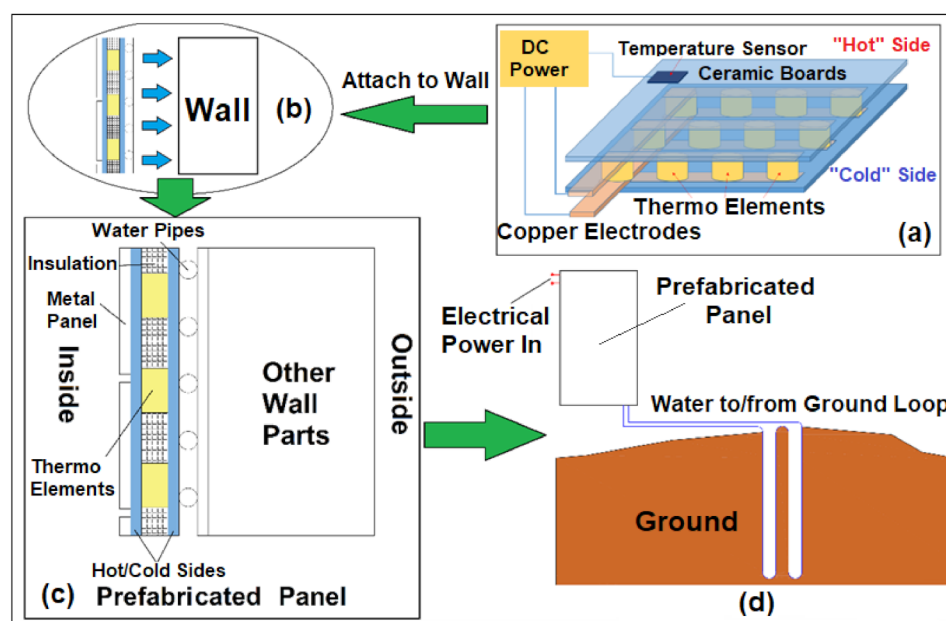


Figure 1. Novel, panelized, ground source, radiant heating and cooling system design for building applications: (a) schematic drawing of the structure of proposed heating/cooling panel, (b) attachment to building envelope component, (c) section view of the prefabricated panel, and (d) connection to the ground loop.

For example, for the TEM system integration with building envelopes, Xu et al. [12] developed an active building envelope system by using commercially available photovoltaic and two types of TEMs, which had good performance during heating/cooling modes. Luo et al. [18] developed a building wall system that integrates TEMs with PhotoVoltaics (PV), whose simulation results show up to 70% daily heat gain reduction, compared to traditional walls on a hot summer day. In their further research study [19], a PV thermoelectric wall system was developed in 2020, which can be used in net-zero energy buildings and had the potential of saving 72–100% energy if utilized in different climate regions,

compared with a regular massive wall. For dehumidification, Irshad et al. [14] evaluated a novel thermoelectric air duct dehumidifier system, which can be used as a good alternative for freshwater production along with the thermal load reduction in buildings in Malaysia. For providing heat to clothes dryers, Patel et al. [16] built a new configuration of clothes dryer in 2021, which can increase the energy efficiency by 6%, and the drying time can be reduced by 47%. For space cooling in buildings, Gillott et al. [5] presented a thermoelectric cooler designed for small-scale space conditioning applications in buildings, whose cooling power can reach up to 220 W. For space heating in buildings, Allouhi [17], in 2017, found that a thermoelectric heating system could help in reducing up to 64% of energy usage in an office room compared to the traditional electric heaters in Morocco. For the development of new TEM heating/cooling units, Riffat et al. [20] developed a computer model to simulate the performance of a novel thermoelectric heat pump system. Koochi et al. [24] proposed a new multipurpose thermoelectric concept that had the potentials to be used in different types of buildings with the goal of optimizing indoor thermal comfort. Siviter et al. [25] designed a new thermoelectric heat pump system for a large power plant, which can help reduce 1.5% fuel usage with the payback year of only 4 years.

Despite the unique advantages of TEMs, the barriers that prevent TEMs from widespread applications are their high initial costs and low energy efficiencies [4,5,11,26,27], especially for their large capacity applications in buildings compared to conventional heating and cooling equipment. For example, He et al. [27] conducted a study of a solar-driven TEM cooling and heating system in a small room, and the average system Coefficient of Performance (COP) for cooling is slightly higher than 0.45. Due to low COPs, TEM systems have therefore been restricted to niche applications [4,11]. High initial costs are considered as another limitation of TEMs. The theoretical optimum design of a thermoelectric cooler for buildings proposed by Riffat and Qiu [26] has a higher initial cost (about three times higher) than a vapor compression air-conditioner with the same output power.

Although TEMs have brought more attention to designers and engineers, making this innovative technology become more viable when deploying into building conditioning systems, the low efficiency [4] and low capacity are still the issue or concern, since most developed systems used ambient air as the heat source or sink; for example, the thermoelectric air-conditioner having the cooling COP of 0.38~0.45 [26], the solar-driven thermoelectric system having a slightly higher cooling COP than 0.45 [27], and the novel thermoelectric refrigeration and space conditioning system mentioned in [28] having the calculated COP of 0.1. This paper, therefore, aims to develop a novel, panelized, ground source, radiant heating and cooling system by utilizing the Peltier effect. The proposed panel system is equipped with water pipes that are attached to one side of the panel and connected with a ground loop to exchange heat between the cold/hot sides of the thermoelectric module and the underground region. The ground loop will be inserted in boreholes and is expected to be the same as those used for a vertical closed-loop Ground Source Heat Pump (GSHP) system, which could be hundreds of feet deep, where the ground temperature is nearly constant. By applying it in buildings and attaching it on building envelope components, such as walls, as a heating and cooling device (Figure 1b,c), the heating and cooling requirements can be met by reversing the voltage (changing the direction of the current) applied on these two sides/substrates. The panels can be prefabricated, and each of them will be equipped with two connections for the electrical power and the ground loop for easy installation (Figure 1d). Like a GSHP system that typically has higher system efficiencies than conventional air-source systems, the proposed system uses the underground region as the heat sink or source and, thus, is expected to have higher system efficiencies compared to other conventional TEM devices that utilize ambient air as the heat sink or source for space cooling or heating in buildings, similar to the concept of using groundwater as the heat sink or source for a thermoelectric heat pump system [29].

2. Materials and Methods

To investigate the performance of the developed panel system, experiments (Figure 2) were conducted in a lab based on the experiment design illustrated in Figure 3. Table 1 shows the parameters of the key devices used in the experiment. As shown in Figure 2, warm or cool water from a water bath/tank used to mimic underground loops flows through the pipes to provide heating or cooling effects to the two heat-exchanging panels made of aluminum. The purchased TEMs are sandwiched between panels. Four of them are grouped together within one heat-exchanging panel with totally two panels (eight TEMs) connected in series by water pipes (Figure 3). The eight TEMs are separated into four parallel electric circuits with two of them in each circuit that are connected electrically in series.

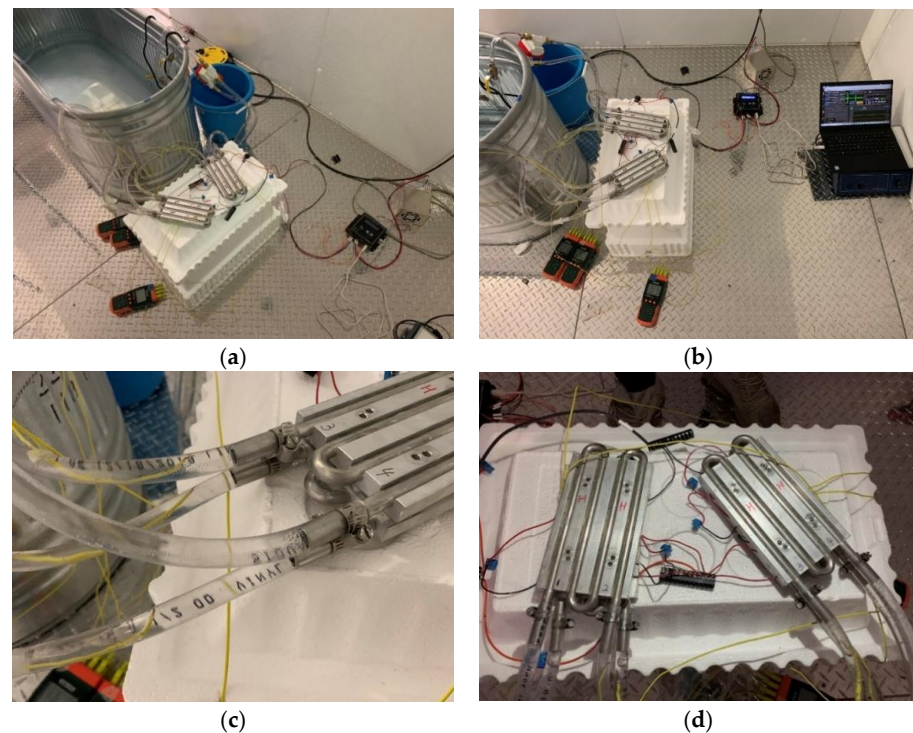


Figure 2. Experiment demonstration: (a,b) overview of the system, (c) water pipes connected with the heat exchanging panels, and (d) heat exchanging panels with the thermoelectric modules in between.

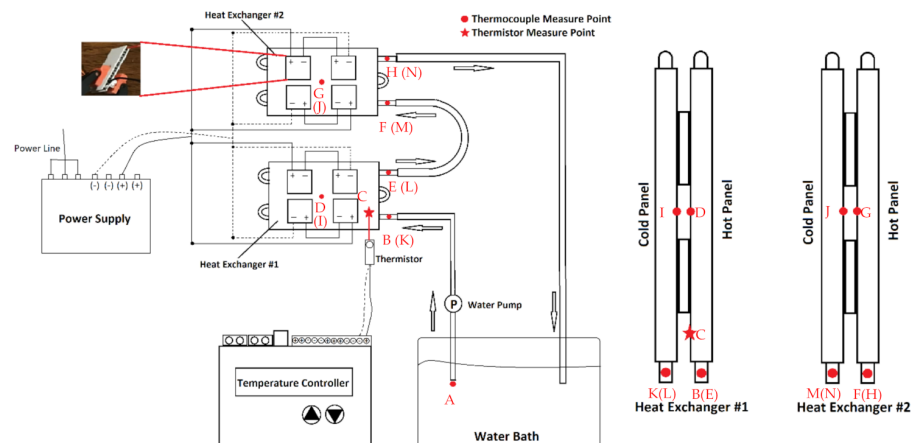


Figure 3. Experiment design (Points A–N: Measurement sensors' locations).

Table 1. Parameters of key experiment components.

Equipment	Parameters
ThermoElectric Module (TEM) *	HP-127-1.4-1.5-72 (127 thermocouples, 40 mm × 40 mm × 3.9 mm)
TEM Seebeck Coefficient * (V/K)	0.0002043 @300 K
TEM Thermal Conductivity * (W/(m·K))	1.458 @300 K
TEM Resistivity * ($\Omega\cdot\text{m}$)	0.103 @300 K
Heat Exchanging Panel *	LC-SSX1(Aluminum, 152.4 mm × 88.9 mm × 12.7 mm)
Temperature Controller *	TC-48-20 (20~100 °C, ± 0.1 °C)
Thermistor *	MP-3193 (−20 to 100 °C, ± 1 °C)
Power Supply *	PS-12-8.4A (85~264 VAC, 12 VDC, 8.5 Amps)
Digital Water Meter **	DM-P-050 (0.0027~0.42 L/s, $\pm 1\%$)
Thermocouple ***	Type-K (−40 to 260 °C, ± 1 °C)
Thermometer Data Logger ***	Extech-SDL-200 (−100 to 1300 °C, ± 1 °C)

* TE Technology [30]. ** Flows [31]. *** Extech [32].

As shown in Figure 3, water from the water bath was supplied by using a constant-volume pump to the two heat exchanging panels one by one at a controlled constant flow rate of 0.17 L/s. Various inlet water temperatures were used at the hot and cold sides of the TEMs to evaluate their performance under different conditions at both the source and load sides of the system. The temperature controller provides additional safety protection for the TEM system to avoid overheating or overcooling by controlling the supplied power through the thermistor located at the inside surface of the hot panel of the heat exchanger #1 (Point C). Thermocouples were used to measure the inlet and outlet water temperatures at Points B, E, F, H, K, L, M, and N as shown in Figure 3. Panel surface temperatures were measured by other thermocouples located at the inside surfaces of the panels, such as Points D, I, G, and J. Water is pumped through heat exchangers' hot and cold panels with the designed inlet water temperatures that vary between around 4.4 °C and 21.1 °C under the given input electrical power (54 W, 120 W, and 266 W) applied on the eight TEMs. The primary limitation of the experiment study is that the inlet water from the water bath as shown in Figure 2, which is exposed to and affected by the ambient air, cannot be controlled precisely to a temperature point that is consistent for all the case studies. For example, Table 2 shows the temperatures of the inlet water supplied to both the cold and hot panels in each case with different input electrical power. Additionally, for each case, panel temperatures, inlet and outlet water temperatures, water flow rates, and the electric power consumed to produce the Peltier effect are measured every second for at least 5~10 min until the measured parameters nearly reach a steady state (almost no change with time). In this study, each experimental case was tested once due to the limited experimental condition involving the inconsistent inlet water temperatures from the water bath, but the mean values of multiple samples (usually more than 100 samples for each case) were used, as the measured parameters became stable, to determine the performance of the system, as well as the uncertainties.

Table 2. Experimental Cases.

Case	Hot Panel				Cold Panel				Input Electrical Power (W)
	Inlet Water Temperature (°C)	Uncertainty			Inlet Water Temperature (°C)	Uncertainty			
		Heating Capacity	Heating COP	Panel Temperature		Cooling Capacity	Cooling COP	Panel Temperature	
1	4.2	1.46%	1.54%	0.78%	4.4	1.64%	1.72%	1.22%	54
2	4.4	1.95%	2.01%	1.60%	4.5	1.35%	1.44%	1.80%	120
3	4.7	1.47%	1.56%	4.62%	4.7	1.87%	1.93%	2.03%	266
4	9.9	1.39%	1.47%	1.67%	4.4	1.61%	1.68%	1.88%	54
5	10.0	1.24%	1.34%	1.17%	4.6	1.52%	1.60%	1.37%	120
6	10.1	1.29%	1.38%	2.48%	4.4	1.67%	1.74%	2.24%	266
7	4.5	1.22%	1.32%	2.59%	21.1	2.56%	2.60%	2.34%	54
8	4.6	1.93%	2.00%	2.89%	21.0	1.15%	1.25%	0.89%	120
9	4.2	2.89%	2.93%	3.25%	20.9	1.35%	1.44%	1.56%	266
10	10.2	3.29%	3.33%	3.27%	21.2	4.35%	4.38%	3.79%	54
11	10.1	1.69%	1.76%	3.23%	20.9	1.95%	2.02%	1.64%	120
12	10.4	1.37%	1.46%	1.99%	20.6	2.27%	2.32%	3.38%	266
13	10.0	1.74%	1.81%	1.82%	14.7	1.49%	1.57%	1.26%	54
14	10.0	2.17%	2.23%	3.61%	14.6	1.36%	1.45%	1.06%	120
15	10.4	1.39%	1.48%	2.80%	14.6	1.41%	1.50%	0.88%	266
16	4.6	1.40%	1.49%	4.81%	14.6	1.49%	1.57%	1.81%	54
17	4.2	3.44%	3.48%	4.40%	14.2	2.18%	2.24%	2.33%	120
18	3.9	2.06%	2.12%	1.31%	14.1	1.44%	1.52%	1.44%	266
19	21.4	1.95%	2.01%	0.72%	4.6	3.51%	3.55%	3.32%	54
20	21.2	3.75%	3.79%	3.40%	4.9	3.75%	3.79%	3.73%	120
21	20.9	1.85%	1.91%	5.36%	4.7	4.49%	4.52%	4.02%	266
22	21.0	2.46%	2.51%	1.83%	14.1	4.53%	4.55%	3.66%	54

Table 2. Cont.

Case	Hot Panel			Cold Panel			Input Electrical Power (W)		
	Inlet Water Temperature (°C)	Uncertainty		Inlet Water Temperature (°C)	Uncertainty				
		Heating Capacity	Heating COP	Panel Temperature		Cooling Capacity	Cooling COP	Panel Temperature	
23	21.0	1.39%	1.47%	1.27%	14.1	4.08%	4.11%	2.66%	120
24	21.1	1.45%	1.53%	4.93%	14.0	2.36%	2.41%	4.36%	266
25	21.4	1.36%	1.45%	1.81%	21.6	1.16%	1.27%	0.68%	54
26	21.3	1.16%	1.26%	0.60%	21.5	1.09%	1.20%	0.40%	120
27	21.3	1.10%	1.20%	0.64%	21.5	1.29%	1.38%	0.40%	266

The use of water at both the source and load sides is to (1) mimic the ground loops that could be buried underground and exchange heat with the underground region, whose temperatures would be $>21.1\text{ }^{\circ}\text{C}$ in hot climates or $<4.4\text{ }^{\circ}\text{C}$ in cold climates across the U.S. [33]; and to (2) provide an easy way to estimate the net heating or cooling effects produced at the hot or cold sides of TEMs, where the heat losses or gains due to the ambient environment were minimized by using insulation materials wrapped around the heat exchanging panels. Figure 4 shows the experimental procedure.

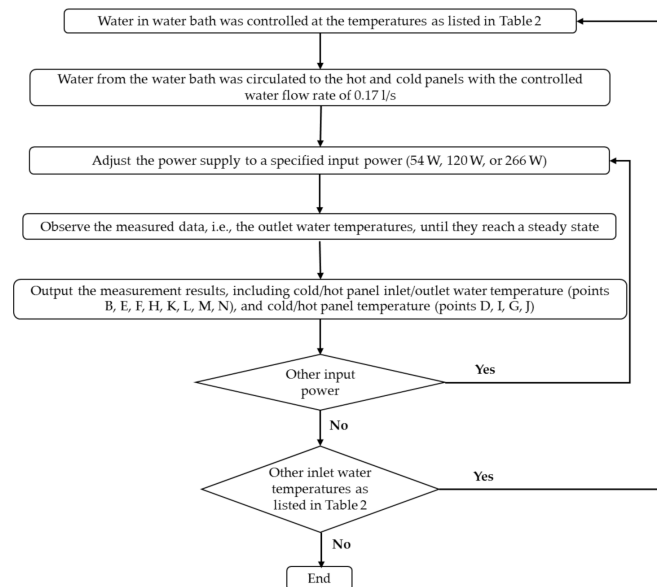


Figure 4. Experimental procedure.

3. Results

The heating/cooling capacity shown in Figures 5 and 6 was determined by using Equation (1), and the corresponding COP was determined by using Equation (2).

$$Q = m_{\text{water}} C_p (T_{\text{in}} - T_{\text{out}}), \quad (1)$$

where Q (W) is the heating/cooling capacity, m_{water} (kg/s) is the mass flow rate of the circulating fluid (water), C_p (J/(kg·K)) is the specific heat capacity of the fluid at constant pressure, T_{in} ($^{\circ}\text{C}$) is the panel inlet water temperature (at Point B or K), and T_{out} ($^{\circ}\text{C}$) is the panel outlet water temperature (at Point H or N).

$$\text{COP} = \frac{Q}{P_i}, \quad (2)$$

where Q (W) is the heating/cooling capacity (from Equation (1)), and P_i (W) is the input power supplied to the TEMs.

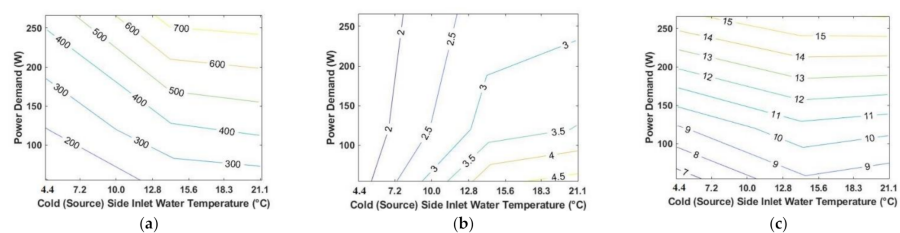


Figure 5. Cont.

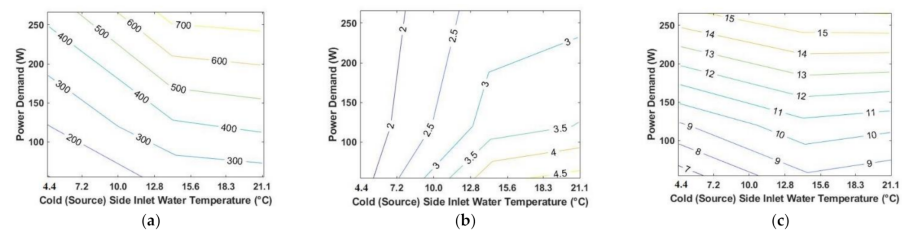


Figure 5. Heating capacities and COPs: (a) Heating Capacity, (b) Heating COPs, and (c) Hot Side Surface T with the hot (load) side inlet water temperature of around 4.4 °C (3.9~4.7 °C); (d) Heating Capacity, (e) Heating COPs, and (f) Hot Side Surface T with the hot (load) side inlet water temperature of around 21.1 °C (20.9~21.4 °C).

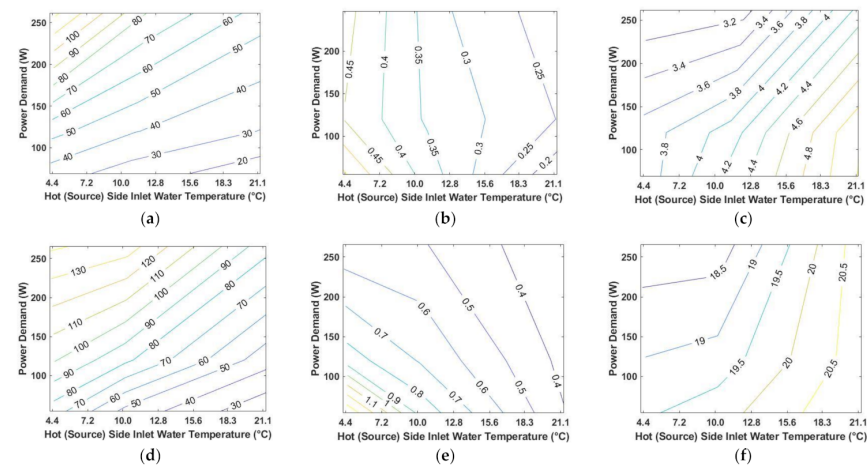


Figure 6. Cooling capacities and COPs: (a) Cooling Capacity, (b) Cooling COPs, and (c) Cold Side Surface T with the cold (load) side inlet water temperature of 4.4 °C (4.4~4.9 °C); (d) Cooling Capacity, (e) Cooling COPs, and (f) Cold Side Surface T with the cold (load) side inlet water temperature of 21.1 °C (20.6~21.6 °C).

Figures 5 and 6 show the heating and cooling performances of the system, respectively, which were extracted from the experimental results. Figure 5 shows the relationships among the electrical power consumed, the inlet water temperatures at the cold (source) side from underground loops, and the heating capacities in W (left figure), COPs (middle figure) or the hot side surface temperatures (in °C) of the panels (right figure), with the given inlet water temperature at the hot (load) side (around 4.4 or 21.1 °C). Figure 6 displays the cooling capacities in W (left figure), COPs (middle figure), and the corresponding cold side surface temperatures (in °C) in the cooling mode of the system (right figure). The heating/cooling capacities were estimated by using the water flow rate and the inlet and outlet water temperatures measured from the two-panel system. The capacity results were then divided by the corresponding electrical power consumed to determine COPs.

The uncertainty was derived from the systematic error and random error [34], both of which were considered in measuring the temperatures, water flow rates, and the electrical powers. The uncertainties for the results shown in Figures 5 and 6 are shown in Table 2, in terms of heating/cooling capacities, COPs, and surface temperatures, where were evaluated by using the uncertainty propagation equations (Equations (3) and (4)) [34].

$$u_C = \left[\sum_{i=1}^L (\theta_i u_{x_i})^2 \right]^{1/2} \quad (3)$$

$$\theta_i = \frac{\partial C}{\partial x_{i, x=\bar{x}}}, \quad i = 1, 2, \dots, L \quad (4)$$

where u_C is the uncertainty; $u_{\bar{x}_i}$ is the instrument uncertainty for each measured variable; θ_i is the sensitivity of uncertainty for measured variables.

In the cooling mode, the cold panel is regarded as the load side, and thus the hot panel is the source side. Otherwise, in the heating mode, the cold panel is regarded as source side, and the load side is the hot panel. As shown in Figure 5, when the load (hot) side inlet water temperature is given, i.e., around 4.4 °C, higher inlet water temperatures at the source side will achieve greater heating capacities if the input power is kept constant. This phenomenon, however, is less prominent when the inlet water temperature is higher than 15.6 °C, i.e., the curves become flat as the inlet water temperature increases. With a given inlet water temperature at the source (cold) side, higher power inputs will achieve greater heating capacities. This indicates that if the inlet water temperatures at the source and load sides, as well as the number of TEMs, in the system are given and remain unchanged, the only way to raise the heating capacity is to increase the power input, i.e., consuming more electrical power, to generate more heating effects. The result also shows that when the inlet water temperature at the source side is low, e.g., 7.2 °C (like the ground temperature in cold climates of the U.S.), the heating COPs will not increase too much as the rise of the input power. When the source-side temperature is high, e.g., 21.1 °C (like the ground temperature in hot climates of the U.S.), higher heating COPs can be achieved, which are more sensitive to the source-side temperature rather than the input power, and the heating COPs increase as the decrease in input powers. For example, under the given conditions in the experiment, the highest heating COP (around 4.5) occurs when the inlet water temperature at the source side is as high as 21.1 °C. This indicates that the proper way to maintain the high efficiency of the proposed system while meeting the heating load of a building is to increase the number of TEMs used in the system, which, apparently, would increase the cost of the system, and therefore finding and/or synthesizing a suitable and affordable thermoelectric material play a significant role.

When the heating load is decreased, i.e., the hot (load) side inlet water temperature increases from around 4.4 °C to 21.1 °C, the heating capacities and COPs are all reduced, and the heating COPs are only sensitive to the cold (source) side inlet water temperature instead of the input power, especially when the input power is higher than a threshold, e.g., 120 W in the experiment. In this case, the corresponding hot-side surface temperatures are around 29.4 °C, which is an ideal surface temperature for the proposed radiant system for space heating, especially if used with a slab as a floor radiant system [35].

For cooling (Figure 6), lower inlet water temperatures at the source (hot) side contribute to the increase in cooling capacities, and when the cooling load is increased, i.e., the cold (load) side inlet water temperature increases from 4.4 °C to 21.1 °C, the cooling capacities and COPs are all increased. Compared to the heating performance, however, cooling COPs are low, which vary between around 0.2 and 1.4. For example, the lowest cooling COP (0.2) occurs when the inlet water temperature at the source side is as high as 21.1 °C and the inlet water temperature at the load side is as low as around 4.4 °C with the given power input of around 266 W, and the highest cooling COP (1.4) occurs when the inlet water temperature at the source side is as low as around 4.4 °C and the inlet water temperature at the load side is as high as around 21.1 °C with the given power input of around 54 W. When the cold (load) side inlet water temperature is around 21.1 °C, the corresponding surface temperatures at the cold side of the panel is around 18.2~21.0 °C, which is a more appropriate temperature set point for the space cooling to avoid the occurrence of condensation on the surface, compared to the other case that has low surface temperatures (<5.3 °C).

Figures 7 and 8 show the details of the heating and cooling COPs of the system, respectively, where Figure 7 shows the relationship between the heating (solid line) and cooling (dashed line) COPs with the given inlet water temperature at the cold (load) side (the horizontal axis), and Figure 8 displays the relationship between the heating (solid line) and cooling (dashed line) COPs with the given inlet water temperature at the hot (load) side (the horizontal axis). The corresponding inlet water temperatures at the hot and cold sides for Figures 7 and 8 are shown in their legends, respectively. For example, the

legend of “COP H: Tin 4.6, 3.9, 4.2” in Figure 7a is for the solid line with three circles (left, middle, and right), where 4.6 °C represents the hot-side inlet water temperature for the circle on the left, and 3.9 °C and 4.2 °C are thus for the circles in the middle and on the right, respectively.

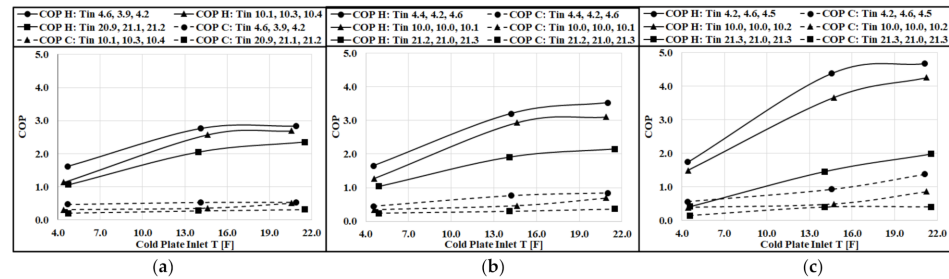


Figure 7. Cold panel inlet water temperature and COPs; (a) power demand: 266 W; (b) power demand: 120 W; (c) power demand: 54 W.

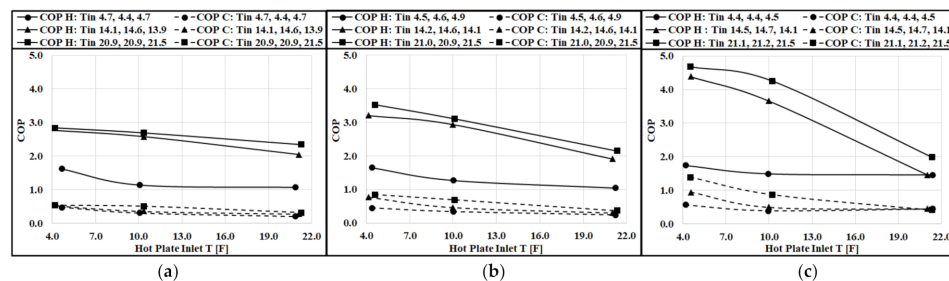


Figure 8. Hot panel inlet water temperature and COPs: (a) power demand: 266 W; (b) power demand: 120 W; (c) power demand: 54 W.

As shown in Figure 7, the input power was decreased from 266 W (Figure 7a) to 54 W (Figure 7c). When the input power is kept constant, the higher heating (solid line) and cooling (dashed line) COPs (dashed line) will be achieved as the given load (cold) side inlet water temperature increases if the hot side inlet water temperature is kept nearly constant. For example, when the inlet water temperature of the cold panel is increased from 4.4 °C to 21.1 °C and the hot panel inlet temperature is around 4.4 °C, the heating COP (solid line with circles) will be increased from 1.8 to 4.7 with the input power of 54 W (Figure 7c). However, when the load (cold) side inlet water temperature is higher than, e.g., 14.5 °C, the curves become flat as the inlet water temperature increase. When the load (cold) inlet water temperature is kept nearly constant, the heating (solid line) and cooling (dashed line) COPs will be increased as the input power is decreased. For example, when the cold panel inlet water temperature is around 21.1 °C and the hot panel inlet water temperature is around 4.4 °C, the heating COPs (the right circle on the solid line) are increased from 2.8 to 4.7, as the input power is decreased from 266 W (Figure 7a) to 54 W (Figure 7c).

As shown in Figure 8, when the input power and cold panel inlet water temperature are kept nearly constant, the higher heating (solid line) and cooling (dashed line) COPs can be achieved as the load (hot) side inlet water temperature decreases. For example, when the input power is 54 W (Figure 8c) and the cold panel inlet temperature is around 21.1 °C, the heating COP (solid line with squares) is decreased from 4.7 to 2.0 if the hot panel inlet temperature is increased from 4.5 °C to 21.3 °C. When the hot and cold panel inlet temperatures are kept nearly constant, the heating (solid line) and cooling (dashed line) COPs are increased as the input power decreases. For example, when the cold panel inlet temperature is kept around 21.1 °C and the hot panel inlet temperature is kept around 4.4 °C, the heating COP (the left square on the solid line) is increased from 2.9 to 4.7 as the input power decreases from 266 W (Figure 8a) to 54 W (Figure 8c). Moreover, at the

constant input power and hot panel inlet temperature, the COPs will be increased as the cold panel inlet temperature is increased.

4. Discussion

For a typical single-family detached house defined by the Pacific Northwest National Laboratory (PNNL) [36], the number of TEMs required to meet the heating and cooling loads of the house is shown in Table 3. The required TEM numbers were determined by using the heating or cooling loads of the house if located in eight different Climate Zones (CZ) across the U.S. designated by the International Energy Conservation Code (IECC) and ASHRAE [37] divided by the heating or cooling capacities of the proposed system, which were determined based on the experimental results (Figures 5 and 6) considering the expected design hot/cold surface temperatures for a radiant system, e.g., 29.4 °C for heating [35] and ~19.4 °C for cooling. The house has two floors with total areas of 334.5 m², where 223.1 m² are the conditioned space, and the window-to-wall ratio is around 14% [36]. Eight cities were selected as the representatives of the eight CZs (Table 3). The effects of local building codes (according to IECC 2021) on the heating and cooling loads of the target building were also considered.

As shown in Table 3, the heating COP decreases as the weather (or the ground) becomes colder from CZ-1 to 8. For example, the heating COP can reach up to 3.17 in hot climates, e.g., in Honolulu, but in cold climates, it is as low as 0.81, e.g., in Fairbanks, due to the relatively cold ground (2.4 °C) compared to 27.2 °C in Honolulu. The developed system will have a heating COP of around 2.0 if used in a region with mild winters and warm grounds, such as CZ-3 or 4. The system will have low cooling efficiencies (up to 0.59, similar to other TEM systems [4,5,26,39]) even though it is used in cold climates, which indicates that the cooling performance of the system cannot be effectively improved by utilizing the ground loop or optimizing the return water temperature. Instead, a new type of thermoelectric material with high $ZT = s^2 / \rho k T$, which can be calculated from the Seebeck coefficient (s), electrical resistivity (ρ), and thermal conductivity (k) with temperatures (T), is expected to be developed or found to further improve it [40,41]. It is also known that the arrangement of the TEMs in cascade would contribute to achieving higher cooling capacities at a comparable efficiency to standard refrigeration techniques [42].

The number of TEMs needed to handle the heating and cooling (sensible) loads was determined by using Equation (5), according to the heating or cooling capacities of the system with eight TEMs (Figure 3) used in the target house located in each climate zone.

$$\text{NO. of TEMs} = \frac{\text{Heating or Cooling Loads}}{\text{Heating or Capacity of the 8 – TEM system}} \times 8 \quad (5)$$

As shown in Table 3, around 75~90 TEMs are needed to heat up the target building in the winters of CZ-1, 2, 3, and 4, and ~180 TEMs are needed for the building located in CZ-8 (Fairbanks). The total TEM costs, i.e., the initial costs to purchase the TEMs needed for space heating or cooling (the last two rows of Table 3), were determined by using Equation (6) with the given TEM unit price [43].

$$\text{Total TEM Cost} = \text{NO. of TEMs} * \text{Unit Price} \quad (6)$$

For the target house, the investment of USD 1900~4500 (TEMs only) in a device for space heating is comparable with the cost of a regular water-to-air heat pump unit based on vapor-compression refrigeration cycles [44] (ductwork costs are not included), especially in hot/warm climates, where higher heating COPs can be achieved. For space cooling, however, more TEMs (around 250~800) are typically needed to cover the entire sensible cooling loads of the target building, which, apparently, make the system unaffordable and not cost-effective. Therefore, additional studies are needed to further improve the cooling performance of the developed system

Table 3. System performance for a single-family house.

		CZ 1	CZ 2	CZ 3	CZ 4	CZ 5	CZ 6	CZ 7	CZ 8
		Honolulu, HI	Tampa, FL	Atlanta, GA	New York, NY	Buffalo, NY	Rochester, MN	International Falls, MN	Fairbanks, AK
	Heating Loads * (W)	6487.45	7007.98	5693.81	5561.81	5069.57	5666.87	4917.65	5477.60
	Cooling Sensible Loads * (W)	5371.70	5634.88	4763.87	4603.27	4237.81	4451.46	4202.35	4585.98
	Heating Capacity ** (W)	680.58	597.65	543.26	499.23	398.12	408.65	281.26	242.56
	Surface T for Heating (°C)	33.54	30.32	29.02	28.05	27.76	27.81	27.45	27.24
	Cooling Capacity ** (W)	54.58	60.56	103.86	130.56	133.00	132.50	135.00	139.00
	Surface T for Cooling (°C)	23.25	21.55	19.60	18.35	18.38	18.36	18.29	18.25
	Ground Temperature *** (°C)	27.17	23.17	17.78	13.61	10.00	10.39	5.78	2.39
	Heating COP **	3.17	2.34	2.17	2.00	1.61	1.66	1.17	0.81
	Cooling COP **	0.21	0.26	0.42	0.53	0.54	0.55	0.56	0.59
NO. of TEMs	To Meet Heating Loads	77	94	84	90	102	111	140	181
	To Meet Cooling Loads	788	745	367	283	255	269	250	264
Total TEM Costs (\$)	To Meet Heating Loads	1901.90	2321.80	2074.80	2223.00	2519.40	2741.70	3458.00	4470.00
	To Meet Cooling Loads	19,463.60	18,401.50	9064.90	6990.10	6298.50	6644.30	6175.00	6520.90

* Heating and cooling loads from [36]. ** With the power input of 250 W. *** Data extracted from GLHEpro [38].

5. Conclusions

This paper aims to develop a novel, panelized, ground source, radiant heating and cooling system by utilizing the Peltier effect. The proposed panel system is equipped with water pipes that are attached to one side of the panel and connected with a ground loop to exchange heat between the cold/hot sides of the thermoelectric module and the underground region. The ground loop is inserted in boreholes and is expected to be the same as those used for a vertical closed-loop GSHP system. Experiments were conducted to evaluate the performance of the proposed system for space heating and cooling, and the conclusions condensed from the experimental results are summarized below.

- The proposed system using the underground region as the heat source has the potential of meeting heating loads of a house while maintaining at a higher system efficiency (up to ~3.0 COP) for space heating compared to conventional heating devices, such as furnaces or boilers, especially in a region with mild winters and relatively warm ground.
- The average cooling COPs of the system are low (0.59 or less) even using the ground as a heat sink, and thus additional studies are needed to improve it.
- The proposed system, however, has other advantages over other conventional heating and cooling systems, which are shown below.
 - It contributes to the achievement of its scalability to larger buildings or applications in different types of buildings since the maximum COP is not dependent on the cooling/heating capacity and geometry factor, as long as the design temperatures at the hot and cold sides and the figure of merit of the thermoelectric material are confirmed [45].
 - It is expected that the developed panel will be prefabricated in shops and thus easily attached to building envelope components, like walls, floors, or ceilings, which is thin (50~80 mm) and light, thus allowing easy and rapid on-site assembly with lower transportation and labor costs.

Although advancement for developing the novel system has been achieved utilizing the Peltier effect and underground boreholes, there remain some limitations on the current study along with unanswered questions and additional research opportunities. For example, the primary limitation of the study involves the use of the water bath/tank to mimic underground loops that could be inserted into boreholes for more than a hundred of meters deep. Some inaccuracies may occur due to the limited experimental condition, e.g., the inlet water temperatures cannot be controlled precisely. It is expected that the experiment conditions will be improved in future studies, e.g., using a large water bath that can precisely control its outlet water temperature. Additionally, some unexpected operating issues may not be able to identify in the current experimental study until field tests can be carried out, where the developed system will be connected with real underground loops. It can be followed with a detailed life cycle cost analysis to verify the results obtained from the lab experiments and to further improve the feasibility of using the proposed system in buildings for heating and cooling.

The existing TEMs use traditional thermoelectric materials, such as bismuth telluride, lead telluride, and half-Heusler alloys [43], which are either expensive or contain toxic elements, making them practically impossible to be used in buildings. VO₂ is an emerging thermoelectric material presenting a large Seebeck coefficient, ~200 to 400 $\mu\text{V}/\text{K}$ at room temperature, and low thermal conductivity, from nearly zero (insulating phase) to 6.9 $\text{W}/(\text{m}\cdot\text{K})$ (metal phase) [46]. These property parameters are comparable to or even better than those of most of the traditional thermoelectric materials, for example, ~175 $\mu\text{V}/\text{K}$ and 1.6 $\text{W}/(\text{m}\cdot\text{K})$, respectively, for bismuth telluride [47]. However, VO₂ uses the earth-abundant element vanadium (V), and therefore the cost of VO₂ would be much lower than that of most of the existing thermoelectric materials containing rare elements, such as Te, Se, Bi, Sb, etc. This makes VO₂ a promising material to form the thermo element of

the proposed thermoelectric heating/cooling panel, which will be investigated further in future studies.

Additionally, more results related to different locations/climates can be included in addition to the eight cities shown in Table 3, which contribute to plotting a high-resolution US map that shows the potential of using the developed system (e.g., the number of TEMs needed) for space heating or cooling of a typical house.

Author Contributions: Conceptualization, Y.Y., Q.Z. and Z.L.; methodology, Y.Y., Q.Z. and Z.L.; investigation, R.M. and X.H.; writing—original draft preparation, Y.Y., R.M. and X.H.; writing—review and editing, A.B. and A.C.M.; visualization, R.M. and X.H.; supervision, Y.Y., Q.Z., Z.L. and A.B.; project administration, Y.Y., Q.Z. and Z.L. All authors have read and agreed to the published version of the manuscript.

Funding: The authors would like to acknowledge the support of the North Dakota State University EPSCoR (No. FAR0032084).

Institutional Review Board Statement: Not applicable.

Informed Consent Statement: Not applicable.

Conflicts of Interest: The authors declare no conflict of interest. The funders had no role in the design of the study; in the collection, analyses, or interpretation of data; in the writing of the manuscript, or in the decision to publish the results.

References

1. IEA. 2021 Global status report for buildings and construction. *United Nations Environ. Programme*. 2021. Available online: <https://www.unep.org/resources/report/2021-global-status-report-buildings-and-construction> (accessed on 22 November 2021).
2. Secretariat, R. Renewables 2020 global status report. *Rep. Paris: REN12*. 2020. Available online: https://www.ren21.net/wp-content/uploads/2019/05/gsr_2020_full_report_en.pdf (accessed on 22 November 2021).
3. Environment and Energy Study Institute (EESI), Fossil Fuels. Available online: <https://www.eesi.org/topics/fossil-fuels/description> (accessed on 22 July 2021).
4. Zhao, D.; Tan, G. A review of thermoelectric cooling: Materials, modeling and applications. *Appl. Therm. Eng.* **2014**, *66*, 15–24. [[CrossRef](#)]
5. Gillott, M.; Jiang, L.; Riffat, S. An investigation of thermoelectric cooling devices for small-scale space conditioning applications in buildings. *Int. J. Energy Res.* **2010**, *34*, 776–786. [[CrossRef](#)]
6. Jangonda, C.; Patil, K.; Kinikar, A.; Bhokare, R.; Gavali, M.D. Review of various application of thermoelectric module. *Int. J. Innov. Res. Sci. Eng. Technol.* **2016**, *5*, 3393–3400.
7. Min, G.; Rowe, D.M. Experimental evaluation of prototype thermoelectric domestic-refrigerators. *Appl. Energy* **2006**, *83*, 133–152. [[CrossRef](#)]
8. Abdul-Wahab, S.A.; Elkamel, A.; Al-Damkhi, A.M.; Is' haq, A.; Al-Rubai'ey, H.S.; Al-Battashi, A.K.; Al-Tamimi, A.R.; Al-Mamari, K.H.; Chutani, M.U. Design and experimental investigation of portable solar thermoelectric refrigerator. *Renew. Energy* **2009**, *34*, 30–34. [[CrossRef](#)]
9. Putra, N.; Sukyono, W.; Johansen, D.; Iskandar, F.N. The characterization of a cascade thermoelectric cooler in a cryosurgery device. *Cryogenics* **2010**, *50*, 759–764. [[CrossRef](#)]
10. Mansour, K.; Qiu, Y.; Hill, C.J.; Soibel, A.; Yang, R.Q. Mid-infrared interband cascade lasers at thermoelectric cooler temperatures. *Electron. Lett.* **2006**, *42*, 1034–1035. [[CrossRef](#)]
11. Zuazua-Ros, A.; Martín-Gómez, C.; Ibañez-Puy, E.; Vidaurre-Arbizu, M.; Gelbstein, Y. Investigation of the thermoelectric potential for heating, cooling and ventilation in buildings: Characterization options and applications. *Renew. Energy* **2019**, *131*, 229–239. [[CrossRef](#)]
12. Xu, X.; Van Dessel, S.; Messac, A. Study of the performance of thermoelectric modules for use in active building envelopes. *Build. Environ.* **2007**, *42*, 1489–1502. [[CrossRef](#)]
13. Liu, Z.; Zhang, L.; Gong, G.; Han, T. Experimental evaluation of an active solar thermoelectric radiant wall system. *Energy Convers. Manag.* **2015**, *94*, 253–260. [[CrossRef](#)]
14. Irshad, K.; Almalawi, A.; Habib, K.; Zahir, M.H.; Ali, A.; Islam, S.; Saha, B.B. Experimental study of a thermoelectric air duct dehumidification system for tropical climate. *Heat Transf. Eng.* **2020**, *42*, 1159–1171. [[CrossRef](#)]
15. Atta, R.M. Solar thermoelectric cooling using closed loop heat exchangers with macro channels. *Heat Mass Transf.* **2017**, *53*, 2241–2254. [[CrossRef](#)]
16. Patel, V.K.; Boudreaux, P.R.; Gluesenkamp, K.R. Validated model of a thermoelectric heat pump clothes dryer using secondary pumped loops. *Appl. Therm. Eng.* **2021**, *184*, 116345. [[CrossRef](#)]

17. Allouhi, A.; Boharb, A.; Ratlamwala, T.; Kousksou, T.; Amine, M.B.; Jamil, A.; Msaad, A.A. Dynamic analysis of a thermoelectric heating system for space heating in a continuous-occupancy office room. *Appl. Therm. Eng.* **2017**, *113*, 150–159. [CrossRef]
18. Luo, Y.; Zhang, L.; Liu, Z.; Wang, Y.; Meng, F.; Wu, J. Thermal performance evaluation of an active building integrated photovoltaic thermoelectric wall system. *Appl. Energy* **2016**, *177*, 25–39. [CrossRef]
19. Luo, Y.; Zhang, L.; Liu, Z.; Yu, J.; Xu, X.; Su, X. Towards net zero energy building: The application potential and adaptability of photovoltaic-thermoelectric-battery wall system. *Appl. Energy* **2020**, *258*, 114066. [CrossRef]
20. Riffat, S.B.; Ma, X.; Wilson, R. Performance simulation and experimental testing of a novel thermoelectric heat pump system. *Appl. Therm. Eng.* **2006**, *26*, 494–501. [CrossRef]
21. Kazmierczak, M.J.; Krishnamoorth, S.; Gupta, A. Experimental testing of a thermoelectric-based hydronic cooling and heating device with transient charging of sensible thermal energy storage water tank. *J. Therm. Sci. Eng. Appl.* **2009**, *1*, 041005. [CrossRef]
22. Yilmazoglu, M.Z. Experimental and numerical investigation of a prototype thermoelectric heating and cooling unit. *Energy Build.* **2016**, *113*, 51–60. [CrossRef]
23. Ibañez-Puy, M.; Bermejo-Busto, J.; Martín-Gómez, C.; Vidaurre-Arbizu, M.; Sacristán-Fernández, J.A. Thermoelectric cooling heating unit performance under real conditions. *Appl. Energy* **2017**, *200*, 303–314. [CrossRef]
24. Koohi, N.; Nasirifar, S.; Behzad, M.; Cardemil, J.M. Experimental investigation and performance assessment of a solar-driven thermoelectric unit for localized heating and cooling applications. *Energy Build.* **2021**, *253*, 111517. [CrossRef]
25. Siviter, J.; Montecucco, A.; Knox, A.R. Rankine cycle efficiency gain using thermoelectric heat pumps. *Appl. Energy* **2015**, *140*, 161–170. [CrossRef]
26. Riffat, S.B.; Qiu, G. Comparative investigation of thermoelectric air-conditioners versus vapour compression and absorption air-conditioners. *Appl. Therm. Eng.* **2004**, *24*, 1979–1993. [CrossRef]
27. He, W.; Zhou, J.; Hou, J.; Chen, C.; Ji, J. Theoretical and experimental investigation on a thermoelectric cooling and heating system driven by solar. *Appl. Energy* **2013**, *107*, 89–97. [CrossRef]
28. Rawat, M.K.; Chattopadhyay, H.; Neogi, S. A review on developments of thermoelectric refrigeration and air conditioning systems: A novel potential green refrigeration and air conditioning technology. *Int. J. Emerg. Technol. Adv. Eng.* **2013**, *3*, 362–367.
29. Mei, V.C.; Chen, F.C.; Mathiprakasam, B. Comparison of thermoelectric and vapor cycle technologies for groundwater heat pump application. *J. Sol. Energy Eng.* **1989**, *111*, 353–357. [CrossRef]
30. TE Technology, Inc. High-Performance Modules. Available online: <https://tetech.com/peltier-thermoelectric-cooler-modules/high-performance/> (accessed on 10 July 2021).
31. Flows. Digital Water Meter—Totalizer and Flow Rate DM Series. Available online: <https://www.flows.com/digital-water-meter-totalizer-and-flow-rate-dm-series/> (accessed on 10 July 2021).
32. Extech. SDL200: 4-Channel Datalogging Thermometer. Available online: <http://www.extech.com/products/SDL200> (accessed on 10 July 2021).
33. ASHRAE. Chapter 34: Geothermal energy. In *ASHRAE Handbook—HVAC Applications, I-P Edition*; ASHRAE: Atlanta, GA, USA, 2015.
34. Figliola, R.S.; Beasley, D. *Theory and Design for Mechanical Measurements*; John Wiley Sons: Hoboken, NJ, USA, 2020.
35. ASHRAE. Chapter 6: Radiant heating and cooling. In *ASHRAE Handbook—HVAC Systems and Equipment, I-P Edition*; ASHRAE: Atlanta, GA, USA, 2020.
36. Department of Energy (DOE). Residential Prototype Building Models. Available online: https://www.energycodes.gov/development/residential/iecc_models (accessed on 10 July 2021).
37. Baechler, M.C.; Williamson, J.L.; Gilbride, T.L.; Cole, P.C.; Hefty, M.G.; Love, P.M. *Building America Best Practices Series: Guide to Determining Climate Regions by County (No. PNNL-17211 Rev. 1)*; Pacific Northwest National Lab (PNNL): Richland, WA, USA, 2010; Volume 7.1.
38. GLHEpro. Available online: <https://hvac.okstate.edu/glhepro.html> (accessed on 10 July 2021).
39. Cheng, T.C.; Cheng, C.H.; Huang, Z.Z.; Liao, G.C. Development of an energy-saving module via combination of solar cells and thermoelectric coolers for green building applications. *Energy* **2011**, *36*, 133–140. [CrossRef]
40. Duan, M.; Sun, H.; Lin, B.; Wu, Y. Evaluation on the applicability of thermoelectric air cooling systems for buildings with thermoelectric material optimization. *Energy* **2021**, *221*, 119723. [CrossRef]
41. Chen, W.H.; Liao, C.Y.; Hung, C.I. A numerical study on the performance of miniature thermoelectric cooler affected by Thomson effect. *Appl. Energy* **2012**, *89*, 464–473. [CrossRef]
42. O'Brien, B.J.; Wallace, C.S.; Landecker, K. Cascading of Peltier couples for thermoelectric cooling. *J. Appl. Phys.* **1956**, *27*, 820–823. [CrossRef]
43. He, J.; Tritt, T.M. Advances in thermoelectric materials research: Looking back and moving forward. *Science* **2017**, *357*, eaak9997. [CrossRef] [PubMed]
44. How Much Does It Cost to Install a Geothermal Heating or Cooling System? HomeAdvisor, Robert Tschudi. 2021. Available online: <https://www.homeadvisor.com/cost/heating-and-cooling/install-a-geothermal-heating-or-cooling-system/> (accessed on 4 November 2021).
45. Riffat, S.B.; Ma, X. Optimum selection (design) of thermoelectric modules for large capacity heat pump applications. *Int. J. Energy Res.* **2004**, *28*, 1231–1242. [CrossRef]

-
46. Lee, S.; Hippalgaonkar, K.; Yang, F.; Hong, J.; Ko, C.; Suh, J.; Liu, K.; Wang, K.; Urban, J.J.; Zhang, X.; et al. Anomalously low electronic thermal conductivity in metallic vanadium dioxide. *Science* **2017**, *355*, 371–374. [[CrossRef](#)] [[PubMed](#)]
 47. Goldsmid, H.J. Bismuth telluride and its alloys as materials for thermoelectric generation. *Materials* **2014**, *7*, 2577–2592. [[CrossRef](#)]